JOURNAL OF AIRCRAFT
Vol. 30, No. 5, Sept.–Oct. 1993

Experimental Study on the Aerodynamic Effects of a Forward-Sweep Angle

Giovanni Lombardi*
University of Pisa, Pisa, Italy

An experimental study to investigate some aerodynamic features of forward-swept wings is described. Pressure distributions on two wing models with different sweep angles ($\Lambda = 0$ deg and $\Lambda = -25$ deg) were evaluated by means of 320 measurement points, up to angles of attack of 28 deg, in low subsonic and transonic regimes. A comparison of the aerodynamic behavior of the two wings, both at low and high angles of attack (stall and poststall conditions) is presented. At low Mach numbers and low angles of attack the experimental data were also compared with numerical results obtained with a panel code. Some characteristics of the forward sweep are discussed and the benefits that can be obtained by applying it in conditions of interference with other lifting surfaces are pointed out.

Nomenclature

b	=	span
C_l	=	sectional lift coefficient
$C_{l\alpha}$	=	low incidence slope of the sectional lift coefficient
C_L	=	wing lift coefficient
$C_{L\alpha}$	=	low incidence slope of the wing lift coefficient
$C_{L\max}$	=	maximum wing lift coefficient
c	=	chord length
c_p	=	pressure coefficient
M	=	Mach number
x	=	distance measured from wing section leading edge
y	=	distance along the span measured from wing root
α	=	angle of attack
α_{st}	=	angle of attack at maximum lift
β_c	=	corrected compressibility factor, $\{1 - [M\cos(\Lambda)]^2\}^{1/2}$
Δc_p	=	pressure coefficient jump across the shock wave
η	=	$y/(b/2)$
Λ	=	angle of sweep, at $\frac{1}{4}$ of the chord

I. Introduction

THE forward-sweep concept is not new, having first been applied during World War II; forward sweep provides the potential for increasing aerodynamic efficiency, improves low speed handling, reduces approach speed, and gives better stall/spin characteristics.[1] However, only recent developments in various technological fields have opened the way to a more extensive use of forward-swept wings. Indeed, the full benefits of this planform could be realized only with the introduction of advanced composite materials, supercritical airfoils, fly-by-wire, and canard configurations (see, for example Refs. 2 and 3); in particular, by using composite materials, the divergence speeds for forward-swept wings can now be substantially increased.[4]

Although some aircraft with such wing geometry operate successfully, there is nevertheless a lack of data to attain a deeper understanding of the real aerodynamic behavior of these configurations; in this work an attempt is made to improve this understanding by analyzing some experimental pressure measurements. In order to assess the relative performance of forward vs unswept wings, tests were performed on two model wings that differ only in the sweep angle: one is unswept, the other has a 25-deg forward sweep. Because the aerodynamic advantages of sweep appear mainly at high angles of attack and transonic speeds, these conditions are investigated in more detail.

Received Oct. 27, 1991; revision received June 1, 1992; accepted for publication June 12, 1992.

*Assistant Professor, Department of Aerospace Engineering, Via Diotisalvi, 2—56126.

II. Forward-Swept Wing

The behavior of an infinite sheared wing is well known,[5] and the results of its analysis can be indifferently applied to backward and forward-swept wings. The main advantages of the sweep are that as the angle of sweep increases, the perturbation velocity varies more slowly with Mach number, and the critical conditions are reached at a higher Mach number. Nevertheless, to have these advantages it is necessary to allow for lower lift values, decreasing with increasing angle of sweep (Λ) in the ratio

$$C_L(\Lambda)/C_L(0) = \cos(\Lambda) \tag{1}$$

The validity of Eq. (1) is limited to incompressible flow; for high subsonic flow the different effects of the compressibility for the two wings should be taken into account. Introducing the corrected compressibility factor β_c and utilizing the Prandtl-Glauert rule, the cosine law [Eq. (1)] can be rewritten as

$$C_L(\Lambda)/C_L(0) = \cos(\Lambda)\beta_c(0)/\beta_c(\Lambda) \tag{2}$$

These very simple formulas, valid for infinite-sheared wings, can be useful for a first evaluation of the global lift coefficient of a swept wing.

Differences between backward and forward sweep arise when three-dimensional effects are considered, particularly at the root, where a "kink" is present, and at the tips. The curved streamlines, typical of the sheared flow, cannot persist into the center or up to the tip; in these regions the streamlines are straightened out. They must be quite straight, for symmetry reasons, in the center plane and also again at some distance from the tips. These features cause the forward-swept wing to have an up-wash at the wing root and a normally lower down-wash at the wing tips. The same curvature of the streamlines produces a boundary layer with a thickness that, for a forward sweep, is larger at the root then at the tips.

All these three-dimensional effects, opposite to those present in backward-swept wings, substantially modify the flow, particularly at the higher angles of attack. Indeed, in these conditions the flow on a forward-swept wing generally separates first in the root region; this suggests the opportunity of including some aerodynamic device in the aircraft, having

a favorable interference effect on the region of the wing where the flow first separates, e.g., a lifting canard or a strake. In any case, to have a real advantage from these interference effects, a deep knowledge of the flow type over the isolated wing is necessary.

III. Experimental Setup

Tests[6] were carried out in the Medium Speed Wind Tunnel of the DAST laboratories, in South Africa. This is a closed circuit pressurized tunnel, with a confined square test section of 1.5-m width and 4.5-m length, enclosed in a plenum. The test section is symmetrically slotted with five tapered "coke bottle" shaped slots per wall, giving a 5% porosity. The airflow in the tunnel is generated by a three-stage axial compressor driven by a 21-MW electric motor; the Reynolds number can be controlled by pressurizing the tunnel. For this experiment, a side wall support with a splitter-plate was used; the mechanism supports the semimodel against the side wall of the tunnel and provides the movement in pitch.

Two flow regimes were chosen for the tests: 1) a low subsonic regime ($M = 0.3$) and 2) a high subsonic regime ($M = 0.7$). By changing the stagnation pressure, the Reynolds number was kept the same ($\sim 2.8 \times 10^6$, referred to the mean aerodynamic chord) at both Mach numbers in order to pinpoint the effects of Mach number variation on the phenomena.

The two wing models, with zero twist and dihedral angles, differ only in their sweep angles ($\Lambda = 0$ deg and $\Lambda = -25$ deg, at $\frac{1}{4}$ of the chord), while their span (0.7 m), aspect ratio (5.7), taper ratio (0.4), and wing sections (NACA 0012) are the same. The models were machined from a 7075 aluminum alloy plate using numerical control technology; on each model pressure ports were fitted to obtain a total of 320 measurement points,[6] with 10 span stations and 32 chord points; the seats for the pressure reading nipples were machined on a five-axis numerical control machine, to ensure that the axes of the pressure orifices were perpendicular to the wing surface. The pressure orifices have a diameter of 0.5 mm. The planforms of the wings, with the location of the pressure orifices, are shown in Fig. 1.

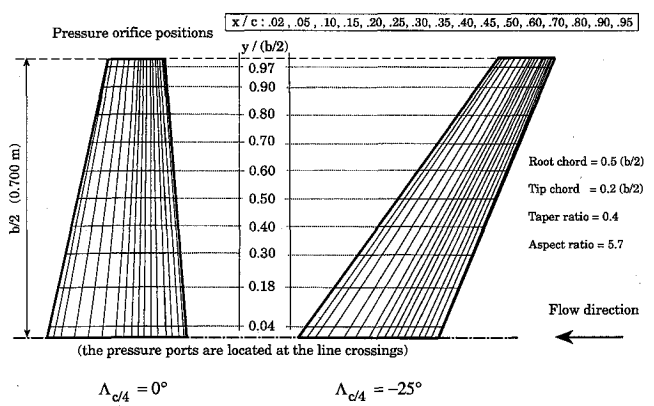

Fig. 1 Plan view of wing models.

The formulation of the error analysis, for both positioning and pressure measurements, has been described in Ref. 6 where the dimensional control carried out on the shape of the wing models and on the position of the orifices is also reported. Strain-gauge measurements carried out at the root of the wing model gave a maximum displacement of 0.0063 mm with a positive change of angle of attack of 0.035 deg (at the tip of the forward-swept model).

Tests were carried out for angles of attack from 0 to 28 deg. The sectional lift coefficient along the span, C_l (nondimensionalized with the dynamic pressure and the local chord) and the global lift coefficient, C_L (nondimensionalized with the dynamic pressure and wing planform surface) were evaluated by means of numerical integration of the pressure distributions.

IV. Discussion of the Results

A. Low Angles of Attack

The global values of the lift curve slope $C_{L\alpha}$ are shown in Table 1 together with the values obtained by means of the incompressible flow panel code FOCAS[7]; the values of the sectional lift slope coefficients along the span $C_{l\alpha}$ are shown in Fig. 2.

The error level in load evaluation, when the panel code is used, is the same for both the forward-swept and the unswept wings. A priori this is not obvious, because with the forward-sweep angle there is a greater influence of the real wake roll-up, not correctly evaluated by a classical panel code which assumes the wake to be plane and fixed. The only zone in which there are some differences is at the root, where a small boundary-layer effect may be present because of the use of semimodels.

At $M = 0.3$ the global values are in rather good agreement with the cosine law [Eq. (1)] for an infinite sheared wing, which is, for the forward-swept wing, 2.4% lower than the experimental result. This difference is related to three-dimensional effects, and then to the up-wash at the root and the down-wash at the tip: since the up-wash is greater (see Sec. II) and acting on a greater surface, a higher lift value in the experiment was really foreseeable. This is confirmed by

Table 1 Slope of the lift curve ($C_{L\alpha}$)

	0.3			
Mach	Experimental	Numerical	Num./ Exp.[a]	0.7
$\Lambda = 0$	0.0786	0.0798	1.0152	0.896
$\Lambda = -25$	0.0730	0.0741	1.0150	0.785
$C_{L\alpha_{\Lambda=-25}}/C_{L\alpha_{\Lambda=0}}$	0.928	0.929		0.876

[a]Numerical/Experimental

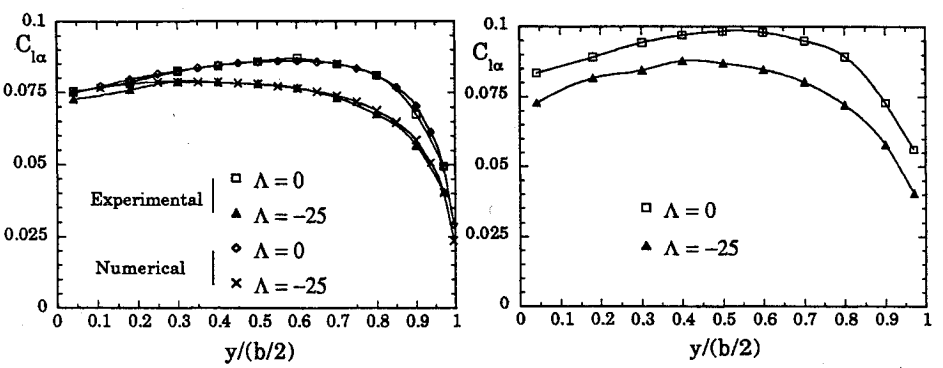

a) $M = 0.3$ b) $M = 0.7$

Fig. 2 Sectional lift slope coefficients along the span.

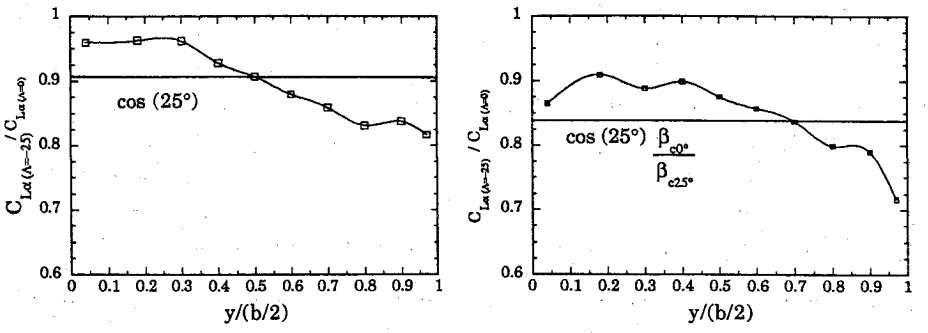

a) $M = 0.3$ b) $M = 0.7$

Fig. 3 Lift ratio between forward-swept and zero-swept wings along the span.

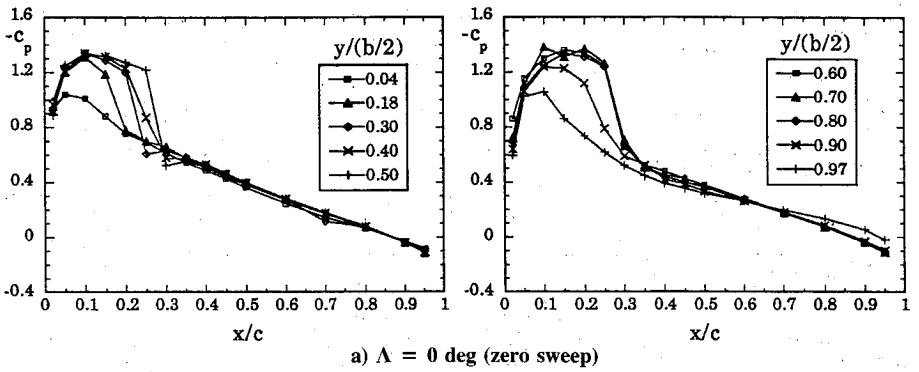

a) $\Lambda = 0$ deg (zero sweep)

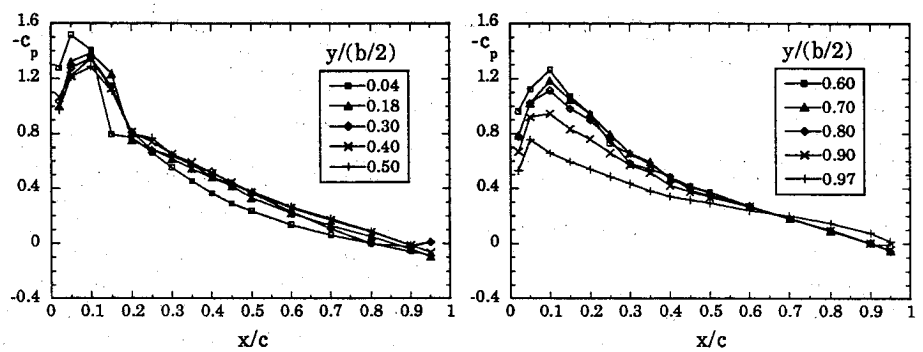

b) $\Lambda = -25$ deg (forward sweep)

Fig. 4 Pressure distributions in chord; $M = 0.7$, $\alpha = 4$ deg.

Fig. 3a, where it is evident that the lift ratio between the forward-swept and the unswept wings is greater than cos(Λ) at the root and lower at the tip.

For a preliminary evaluation at $M = 0.7$ we can utilize Eq. (2), and the result is again lower than the experimental one (4.6%). The difference is clearly greater at the higher subsonic Mach number, but the qualitative three-dimensional effects are similar to those at $M = 0.3$ (Fig. 3b).

At $M = 0.7$ shock waves in the field even at low angles of attack are present, and the behavior is different for the two wing planforms. Figure 4 shows the pressure distributions on the upper surface, for $\alpha = 4$ deg, at several stations $\eta = y/(b/2)$ along the semispan. On the unswept wing, a well-identifiable shock wave is present from η 0.15 to 0.85; the position in chord, between 25–30%, and the intensity ($\Delta c_p \approx 0.6$) are almost constant. On the contrary, only a small shock wave is present on the forward-swept wing, from the root to $\eta \approx 0.25$, and with a lower intensity ($\Delta c_p \approx 0.5$).

B. High Angles of Attack

In Fig. 5 the C_L-α curves for $M = 0.3$ are shown; the values of maximum lift coefficients ($C_{L\max}$) and corresponding angles of attack (α_{st}) are reported in Table 2. The forward-swept wing has a maximum lift coefficient that is lower but close to that of the unswept wing; however, this value is reached at a much higher angle of attack. This stall behavior confirms previous available results.[8]

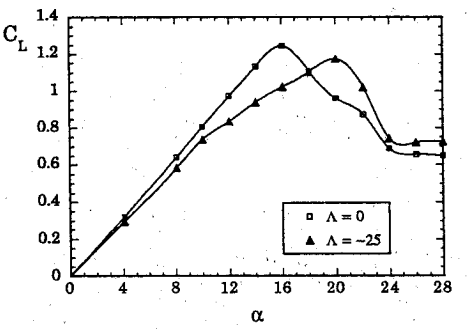

Fig. 5 C_L-α curves; $M = 0.3$.

Table 2 Stall conditions for $M = 0.3$

Λ	$C_{L\max}$	α_{st}, deg
0	1.245	15.8
−25	1.173	19.8

The considerable difference in stall behavior can be appreciated from Fig. 6, where the C_l-α curves for several span stations are reported. The stall of the unswept wing is con-

siderably uniform along the span, as regarded by both the angle of attack (slightly smaller than 16 deg, which is the stall angle for the NACA 0012 airfoil[9]), and the lift coefficient (which, conversely, is much smaller than the maximum C_L of the wing section). The stall is at higher angles of attack only very close to the tip ($\alpha_{st} \approx 20$ deg at $\eta = 0.97$). On the contrary, in the forward-swept wing, the sections near the root reach the stall conditions at a very low angle of attack, with very low lift coefficients ($\alpha_{st} \approx 14$ deg with $C_l \approx 0.7$ at $\eta = 0.04$); moving from the root to the tip, the stall conditions

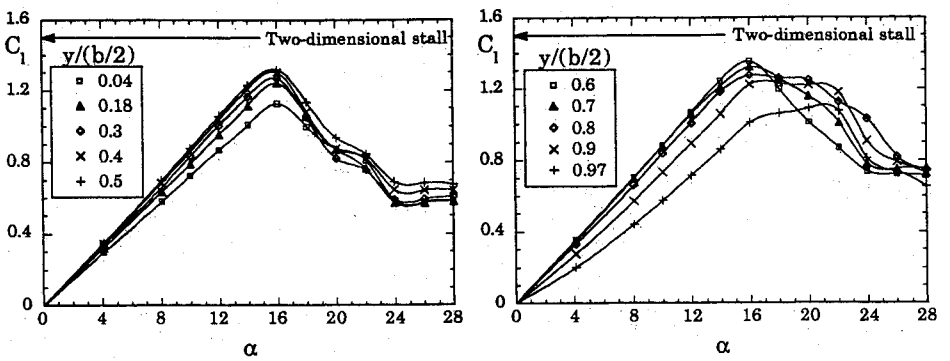

a) $\Lambda = 0$ deg (zero sweep)

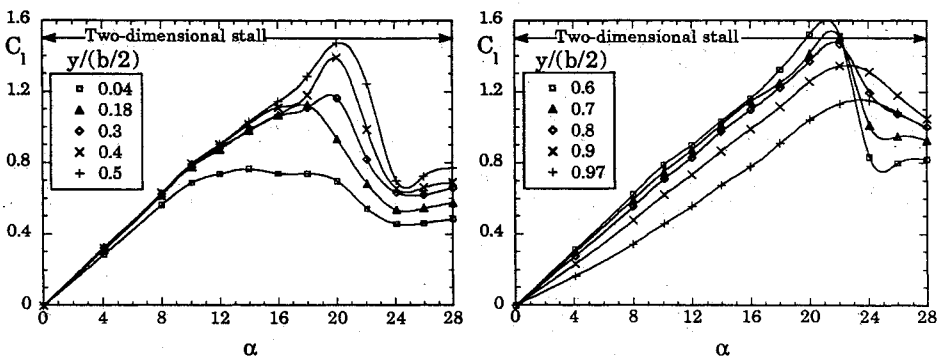

b) $\Lambda = -25$ deg (forward sweep)

Fig. 6 C_l-α curves for several span stations; $M = 0.3$.

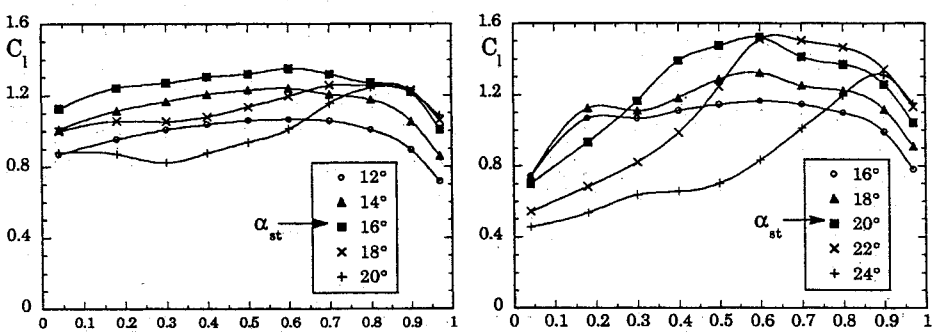

a) $\Lambda = 0$ deg b) $\Lambda = -25$ deg

Fig. 7 Spanwise C_l curves near stall and poststall; $M = 0.3$.

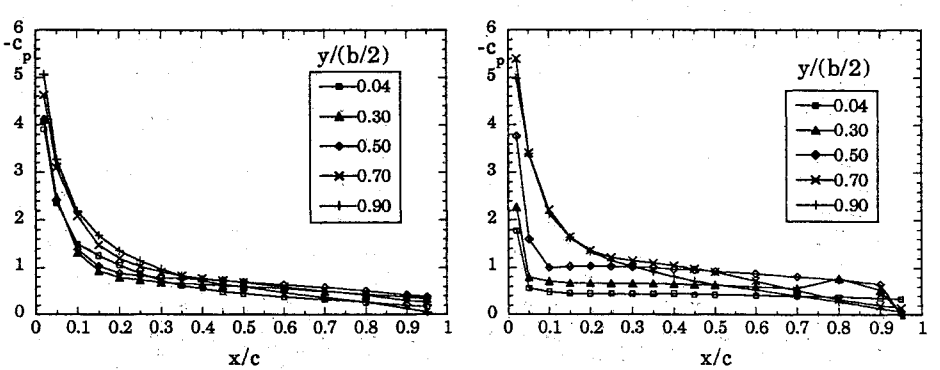

a) $\Lambda = 0$ deg; $\alpha = 18$ deg b) $\Lambda = -25$ deg; $\alpha = 22$ deg

Fig. 8 Pressure distributions in chord beyond α_{st}; $M = 0.3$.

Table 3 Stall conditions for $M = 0.7$

Λ	$C_{L\max}$	α_{st}, deg
0	0.702	11.5
−25	0.677	11.3

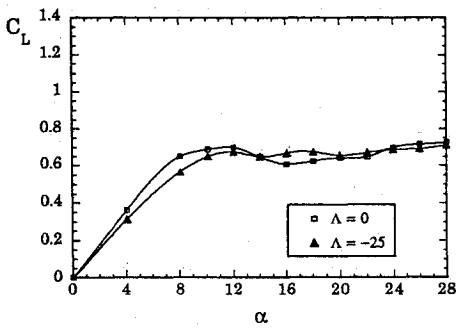

Fig. 9 C_L-α curves; $M = 0.7$.

are reached at higher angles of attack ($\alpha_{st} \approx 24$ deg at $\eta = 0.97$) with high sectional lift coefficients ($C_l \approx 1.6$ at $\eta = 0.6$) which, for η between 0.6–0.8, are higher than the airfoil maximum lift coefficient. This stall behavior is consistent with the forward-sweep flow delineated in Sec. II, and implies a pressure center moving towards the tip (see Fig. 7b); on the other hand, the zero-sweep stall features a shorter displacement of the pressure center towards the tip (see Fig. 7a). It is important to note that the stall observed for the forward-swept wing is opposite to that typical of a swept-back wing.[10]

A further difference can be found in the poststall behavior; the zero-sweep stall is a "soft" one, while the forward-sweep stall is "sharper." This difference is a consequence of the type of flow near the stall condition. As in the unswept wing, all sections have the same local stall angle of attack (see Fig. 6a), beyond this angle each section again exhibits a partially attached flow (see Fig. 8a, which shows pressure distributions on the upper surface at an angle of attack of 18 deg, 2.2 deg greater than α_{st}), so that there is a slow global lift decrease. On the contrary, in the forward sweep at the angle of attack corresponding to the maximum global lift, a large region of

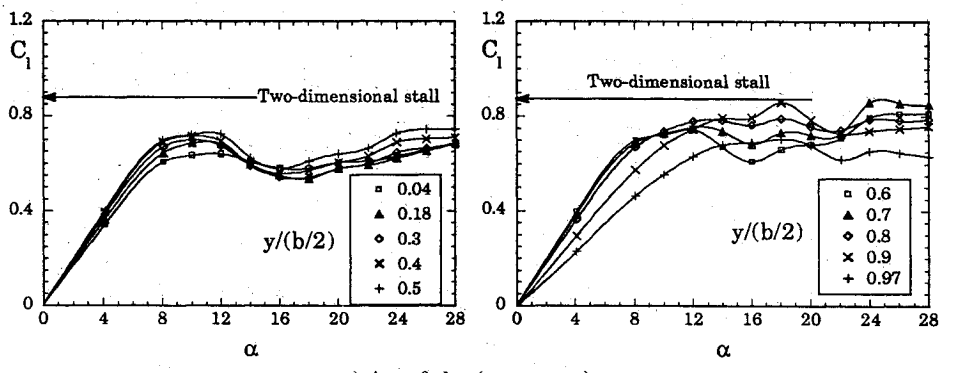

a) $\Lambda = 0$ deg (zero sweep)

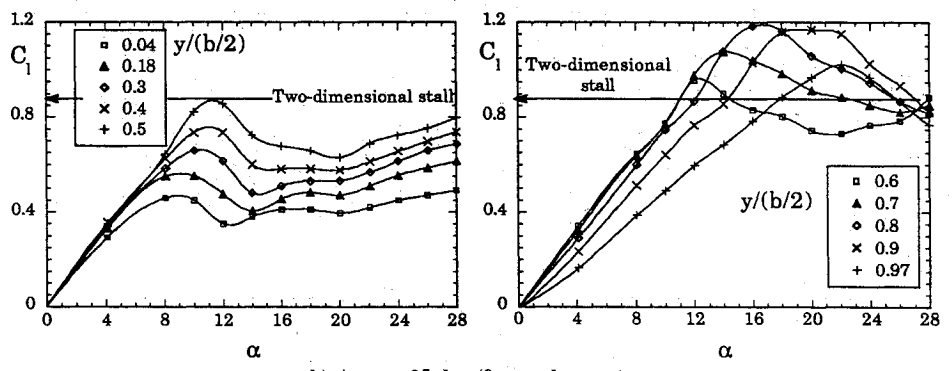

b) $\Lambda = -25$ deg (forward sweep)

Fig. 10 C_l-α curves for several span stations; $M = 0.7$.

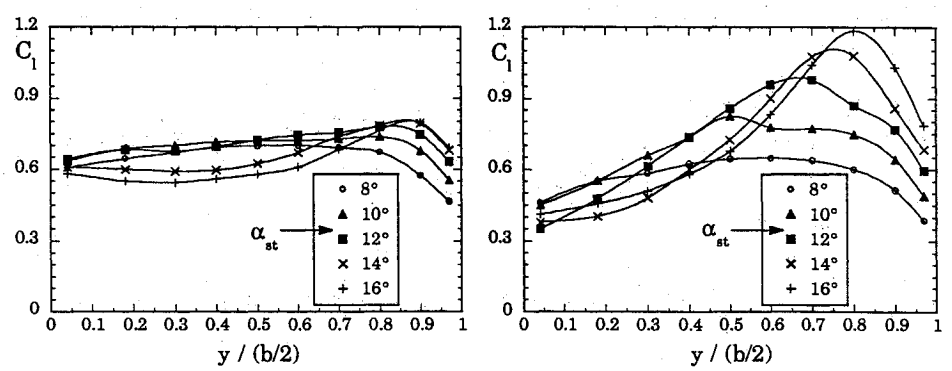

a) $\Lambda = 0$ deg **b) $\Lambda = -25$ deg**

Fig. 11 Spanwise C_l curves near stall and poststall; $M = 0.7$.

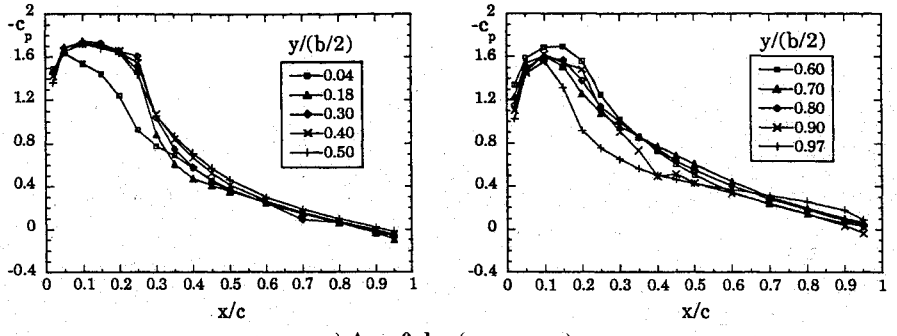

a) Λ = 0 deg (zero sweep)

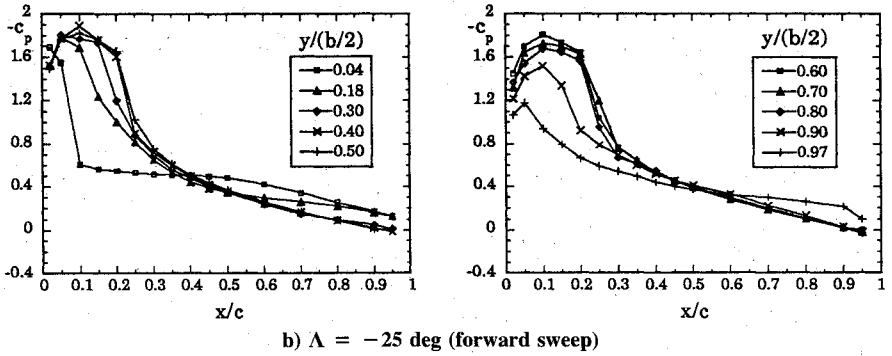

b) Λ = −25 deg (forward sweep)

Fig. 12 Pressure distributions in chord; $M = 0.7$, $\alpha = 8$ deg.

the wing is already stalled (see Fig. 6b), so that beyond this angle the flow is almost fully separated (see Fig. 8b, which shows pressure distributions on the upper surface at an angle of attack of 22, 2.2 deg greater than α_{st}), with a consequent faster lift decrease. However, in both cases, there is a delay in the stall near the tip (see Figs. 6–8); this suggests the presence of a considerable tip-vortex also over the stall conditions.

In Fig. 9 the C_L-α curves for $M = 0.7$ are shown; the values of maximum lift coefficients and corresponding angles of attack are reported in Table 3. In the high subsonic regime the maximum lift values are much lower for both the wings, and the stall conditions are reached at very low angles of attack; it should be remembered that the wing section is not particularly suited for transonic flow, so that compressibility effects are amplified. The analysis of Fig. 9 and Table 3 suggests that at high subsonic Mach numbers the aerodynamic behavior at high angles of attack of the two wing planforms is similar; however, this is true only for the global values, because it is clear from Fig. 10, where the C_l-α curves for several span stations are reported, that the stall type is again different. As for the low subsonic regime, along the span the zero-sweep stall is the same regarding both angle of attack and lift coefficient, the latter very much lower than the maximum life coefficient of the wing section (assumed to be equal to 0.875[11]), whereas, in the forward-swept wing the sections near the root reach the stall conditions at a very low angle of attack with very low lift coefficient ($\alpha_{st} \approx 8$ deg with $C_l \approx 0.45$ at $\eta = 0.04$). In the forward-swept wing, moving from the root to the tip, the stall conditions are reached at higher angles of attack, with high sectional lift coefficients ($\alpha_{st} \approx 20$ deg with $C_l \approx 1.18$ at $\eta = 0.90$); the latter are higher than the two-dimensional ones for $\eta > 0.6$. This behavior is similar to the subsonic one, with a slightly lower uniformity in the spanwise stall of the zero-swept wing, and a much higher difference between root and tip stall conditions for the forward-swept wing (see Fig. 11). This aspect of the transonic flow can be explained by analyzing the spanwise shock waves developing at angles of attack near the stall conditions. Figure 12 shows, e.g., the pressure distributions on the upper surface for $\alpha = 8$ deg at several stations along the span. In the unswept wing the shock-wave is not clearly defined, its position is about 30% in the chord direction, with an intensity that decreases from $\Delta c_p \approx 0.8$ at $\eta = 0.18$ to $\Delta c_p \approx 0.4$ at $\eta = 0.70$. This produces an anticipated separation in the root region, because of the stronger shock wave interaction with the boundary layer. On the contrary, a well-defined shock wave is present on the forward-swept wing, particularly at the root ($\Delta c_p \approx 1$ at $\eta = 0.04$) and with a lower, almost constant value ($\Delta c_p \approx 0.8$), from $\eta \approx 0.15$ to $\eta \approx 0.85$; at the root the shock-wave position is more advanced (from 5 to 10% of the chord), and it moves back, about 20–30%, approaching the tip. The very strong shock wave present at the root produces a separated flow that practically affects the entire wing chord because of the advanced position of the shock. Furthermore, in transonic flow, the stall conditions are more anticipated in the forward-swept wing compared to the $M = 0.3$ case, and this accounts for the nearly equal values of Table 3. The described stall behavior implies a pressure center moving similarly to the low subsonic regime.

The analysis of the global values (see Fig. 9) suggests that at $M = 0.7$ there is a soft poststall for both wings; but, whereas for the unswept wing this is true for almost the whole span, for the forward-swept wing it is only an "integral" consequence of a flow completely attached in some regions, and almost fully separated in other regions (Fig. 10).

V. Conclusions

An experimental study on the behavior of forward-swept wings has been described. In spite of the limited number of analyzed configurations, these results show that at low angles of attack the aerodynamic behavior of a forward-swept wing is close to that foreseeable from the analysis of the expected flow pattern. Therefore, in these conditions, a first evaluation of the lift by means of very simple methods can be considered, and the lift distribution can be evaluated by a panel method as accurately as in more classical planforms.

At high angles of attack the forward-swept wing behavior is very different from the unswept one. The qualitative difference is again foreseeable from the analysis of the expected flow patterns. These differences, and in particular the different regions of separated flow, are to be accurately taken into account when high-lift devices and stall control approaches

are considered; it is clear that they cannot be studied with the same criteria utilized for unswept (or backward-swept) wings. At the high Mach numbers on the forward-swept wing, a strong and advanced shock-wave is present at the wing root; it is probably caused by the kink that produces a stronger and more advanced negative pressure peak. The presence of this strong shock wave should be taken into account when a forward-sweep configuration is considered.

With the selected taper ratio, a considerable departure from the elliptical lift distribution can be observed on the forward-swept wing with a consequent increase in vortical drag; to reduce this disadvantage it is necessary to either increment the taper ratio or to modify the twist.

From the aerodynamic viewpoint, the lift distribution acting on a forward-swept wing, particularly at high angles of attack, can be turned to a real advantage if coupled with a canard control surface. In these conditions the canard wake induces a down-wash at the wing root and an up-wash at the wing tip, so that for tapered wings the lift distribution becomes nearer to the elliptical type and more uniform stall conditions along the span may be obtained. For these configurations it is possible (taking into account flight mechanics considerations) to select parameters (wing and canard geometry and respective position) allowing significant advantages in drag and stall behavior; in this regard the forward sweep is superior to the backward sweep, for which effects of this type are impossible.

Acknowledgments

The author wishes to thank the Division of Aeronautical System Technology, of the CSIR South Africa, for the experimental data in this article which were acquired through a collaboration project carried out by Ing. M. Morelli and support staff in their Medium Speed Wind Tunnel. Thanks are also due to G. Buresti, of the Aerospace Engineering Department of University of Pisa for his guidance and many helpful discussions.

References

[1]Ricketts, R. H., and Doggett, R. V., "Wind-Tunnel Experiments on Divergence of Forward-Swept Wings," NASA TP-1685, Aug. 1980.

[2]Spact, G., "The Forward Swept Wing: A Unique Design Challenge," AIAA Paper 80-1885, Aug. 1980.

[3]Mann, M. J., "A Forward-Swept-Wing Fighter Configuration Designed by a Transonic Computational Method," *Journal of Aircraft*, Vol. 23, No. 6, 1986, pp. 506–512.

[4]Krone, N. J., Jr., "Divergence Elimination with Advanced Composites," AIAA Paper 75-1009, Aug. 1975.

[5]Kucheman, D., "The Aerodynamic Design of Aircraft," Pergamon, London, 1978, pp. 103–220.

[6]Buresti, G., Lombardi, G., and Morelli, M., "Pressure Measurements on Different Canard-Wing Configurations in Subsonic Compressible Flow," Atti del Dipartimento di Ingegneria Aerospaziale, Univ. of Pisa, ADIA 91-4, Pisa, Italy, Sept. 1991.

[7]Polito, L., and Lombardi, G., "Calculation of Steady and Unsteady Aerodynamic Loads for Wing-Body Configurations at Subcritical Speeds," Vol. 1, *AIDAA Conference Proceedings*, Napoli, 1983, pp. 209–222.

[8]Buresti, G., and Lombardi, G., "Indagine Sperimentale Sull'Interferenza Ala-Canard," *L'Aerotecnica, Missili e Spazio*, Vol. 67, Nos. 1–4, 1988, pp. 47–57.

[9]Abbott, I. K. and Von Doenhoff, A. E., "Theory of Wing Sections," Dover, 1959, p. 462.

[10]Furlong, G. C., and McHugh, J. G., "A Summary and Analysis of the Low-Speed Longitudinal Characteristics of Swept Wings at High Reynolds Number," NASA Rept. 1339, 1957.

[11]"Maximum Lift Coefficients for Airfoil Sections at Mach Numbers from 0.6 to 0.75," Emergency Services Data Unit, ITEM W.01.01.07.